THE JOURNAL OF PHYSICAL CHEMISTRY A
A JOURNAL OF THE AMERICAN CHEMICAL SOCIETY

pubs.acs.org/JPCA Article

Computational Investigations of the Lithium Superoxide Dimer Rearrangement on Noisy Quantum Devices

Qi Gao,* Hajime Nakamura, Tanvi P. Gujarati, Gavin O. Jones, Julia E. Rice, Stephen P. Wood, Marco Pistoia, Jeannette M. Garcia,* and Naoki Yamamoto*

Cite This: J. Phys. Chem. A 2021, 125, 1827−1836 Read Online

ACCESS | Metrics & More | Article Recommendations | Supporting Information

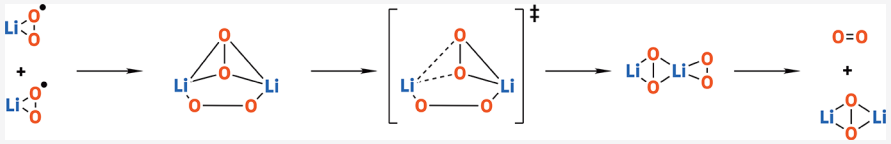

ABSTRACT: Quantum chemistry studies of biradical systems are challenging due to the required multiconfigurational nature of the wavefunction. In this work, Variational Quantum Eigensolver (VQE) is used to compute the energy profile for the lithium superoxide dimer rearrangement, involving biradical species, on quantum simulators and devices. Considering that current quantum devices can only handle limited number of qubits, we present guidelines for selecting an appropriate active space to perform computations on chemical systems that require many qubits. We show that with VQE performed with a quantum simulator reproduces results obtained with full-configuration interaction (Full CI) for the chosen active space. However, results deviate from exact values by about 39 mHa for calculations on a quantum device. This deviation can be improved to about 4 mHa using the readout mitigation approach and can be further improved to 2 mHa, approaching chemical accuracy, using the state tomography technique to purify the calculated quantum state.

1. INTRODUCTION

Quantum computing is a method of computation that possesses the potential to surpass conventional computing (so-called classical computing). While the theoretical framework governing quantum computing has been established for decades, and algorithms have been developed for a variety of application areas, the field has recently experienced a surge in interest due to newly demonstrated success in manufacturing qubit devices. However, device technology is still in its infancy, and the quantum devices currently in operation, known as noisy intermediate-scale quantum (NISQ)[1] devices, depend on hybrid approaches involving the use of qubits in combination with classical computing architectures.

Quantum computing possesses enormous near-term potential for the development of applications in a number of areas, including quantum chemistry, for which finding eigenvalues of eigenvectors is an intractable problem for classical computers. Quantum computing may be particularly effective for such problems, and algorithms such as quantum phase estimation (QPE)[2] and the Variational Quantum Eigensolver (VQE)[3] have been developed to find eigenvalues for approximate, but highly accurate, solutions to the Schrödinger equation. VQE, in particular, is a hybrid classical/quantum algorithm, which, due to a comparatively shorter circuit than QPE, reduces time requirements for qubits to remain coherent, and has been effectively utilized to perform quantum chemistry calculations on noisy quantum devices.[4]

A notable application of VQE has been demonstrated by combination with heuristic trial wavefunctions designed for state preparation in investigations of the ground state (GS) dissociation profiles of hydrides on a quantum device.[4] Those calculations demonstrated that energies computed for dissociation profiles on quantum devices are nearly similar to those computed with a classical matrix eigenvalue decomposition method (full-configuration interaction, or Full CI, or FCI) for the hydrogen molecule, but profiles deviate significantly from chemical accuracy for distances far from the equilibrium geometries of lithium hydride (LiH) and beryllium hydride (BeH_2). Later, an error mitigation protocol was utilized to study dissociation profiles for the H_2 and LiH molecules,[5] but this technique resulted in errors ranging from 60 to 70 mHa, which are much larger than the desired chemical accuracy of 1.6 mHa.

Although those pioneering investigations validate the possibilities of using quantum computing on applications of real-world interests in chemistry, there are a few fundamental issues associated with performing VQE on a noisy quantum device that will need to be addressed. One issue is related to

Received: October 21, 2020
Revised: February 10, 2021
Published: February 26, 2021

https://dx.doi.org/10.1021/acs.jpca.0c09530
J. Phys. Chem. A 2021, 125, 1827−1836

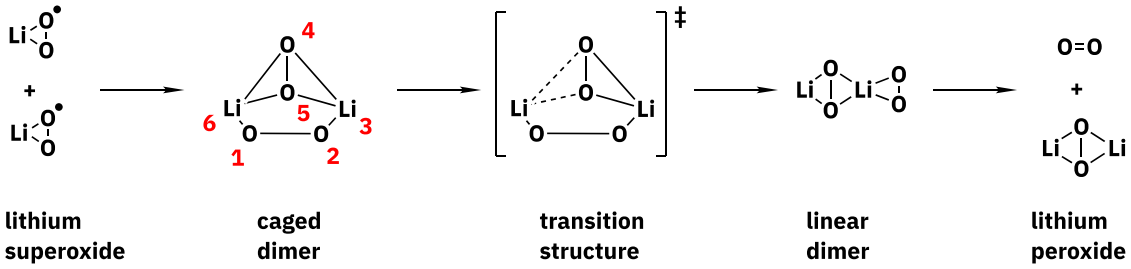

Figure 1. Formation of lithium peroxide and molecular oxygen via the rearrangement of caged lithium superoxide dimer into linear superoxide dimer.

validation of results derived from performing simulations with the VQE algorithm. Previous benchmarks of VQE involved simple molecular systems such as the hydrogen, lithium hydride, and water molecules,[4−6] which can be accurately calculated by computationally inexpensive single-reference ab initio methods like Hartree−Fock (HF) and density functional theory (DFT). However, very few surveys have been performed with VQE on more complicated chemical processes, such as those involved in investigations of reaction mechanisms involving bond formation or bond breaking in transition states, conical intersections caused by intersections between potential energy surfaces (PES), and the generation of species with other complex electronic structures such as radicals, carbenes, and radical ions.[7,8] To evaluate the applicability of the VQE algorithm for its general use in quantum chemistry investigations, one must assess systems that require descriptions of the electronic states by multireference ab initio techniques.

The accuracy one can expect in the current era of quantum computing is limited by noise. Though promising error mitigation approaches have been proposed, order-of-magnitude lower error rates are still required to achieve chemical accuracy.[5,9] Moreover, most error mitigation approaches only focus on error rates derived from readout mitigation or noise extrapolation, but there has been a dearth of research on the purity of the quantum state, which is necessary for calculations of excited states and molecular properties.[6,10]

This manuscript describes an application of the VQE algorithm for the investigation of the rearrangement of the lithium superoxide dimer, which requires an accurate description of bond breaking and formation through a transition state by multireference ab initio methods to obtain an accurate potential energy surface.

This reaction is potentially involved in the discharging process in lithium−air (Li/O_2) batteries, which possess higher energy densities than widely used lithium-ion batteries.[11−15] During discharge, lithium combines with superoxide, formed from the reduction of oxygen at the cathode, to produce lithium peroxide (Li_2O_2) via a lithium superoxide ($LiO_2^{\bullet}$) intermediate.[16−18] Interestingly, lithium superoxide may also dimerize to generate lithium peroxide plus an oxygen molecule via a rearrangement process (Figure 1).[17,18] The overall effect of these processes is that molecular oxygen is consumed at the lithium cathode during discharge to produce lithium peroxide and regenerate residual oxygen gas. We note that since the lithium superoxide dimer has a biradical structure in which singlet and triplet states are necessarily a superposition of two electronic configurations,[17] multireference ab initio methods are required to correctly describe the electronic state. Previous quantum chemistry studies of the lithium superoxide dimer reaction mechanism have demonstrated that DFT, a widely used approach for exploring potential energy surfaces, is inadequate and that correlation provided by the coupled cluster singles and doubles (CCSD) method, or better, is necessary.[17] Therefore, we aim to clarify whether VQE can accurately predict the reaction mechanism for the lithium superoxide dimer rearrangement and to demonstrate how one can obtain chemically accurate results on quantum devices. In particular, we propose an error mitigation scheme based on purification of the quantum state to obtain a pure state with an energy very close to that of the ground state.

To use a noisy quantum device to perform quantum chemistry calculations on molecules such as those of interest to this investigation, one has to ensure that the number of logical qubits are available depending on the problem of interest. The number of qubits (which map directly to the number of spin orbitals of molecules) required for this problem is 60 for the full set of atomic orbitals with a minimal basis set, or 48, if core orbitals, which may be reliably neglected since they do not interact with valence orbitals, are frozen. At present, however, the number of qubits that can reliably be used for computation are limited. Consequently, further qubit reductions need to be employed to make use of such noisy quantum devices for investigations such as the one that we focus on in this manuscript. We demonstrate that the reduction of orbitals to a set of active orbitals that provide a reliable description of the static electron correlation during the dimer rearrangement process can effectively reduce this problem down to the few qubits required to perform calculations on quantum devices[19−27] by first evaluating the important determinants classically. To our knowledge, this is the first demonstration of such a protocol to a reaction occurring in the lithium−air battery. We show that it is feasible to reduce the active space down to one comprising six spin orbitals while preserving a correct description of the potential energy surface that describes a potential reaction pathway. This strategy enables us to conduct experiments with superconducting quantum devices to simulate the chemical rearrangement process.

Using the active space obtained through the above procedure, the potential energy surface is calculated using the VQE algorithm on a quantum simulator and quantum devices using the selected active space. Results from quantum simulation reproduce the exact values even for the system in which two valence electrons occupy two degenerate orbitals, i.e., the energy levels of singlet and triplet states are almost equivalent. On the other hand, due to device noise, results derived from simulations on quantum devices are approximately 39 mHa higher than the exact values. The accuracy of results derived from the use of the VQE algorithm is improved by an order of magnitude using the readout error mitigation

https://dx.doi.org/10.1021/acs.jpca.0c09530
J. Phys. Chem. A 2021, 125, 1827−1836

approach. However, the error is still larger than required chemical accuracy by a factor of 2−3 and the quantum state derived from the use of this approach is still a mixed state. We have successfully improved these accuracies to about 2 mHa on a quantum device by utilizing an error mitigation scheme that utilizes quantum state tomography, which provides a pure state from VQE calculations.

Our approach involving the selection of an appropriate active space and purification of the quantum state makes it possible to use VQE to perform quantum computations on noisy devices with high accuracy on larger-scale chemical reactions requiring the use of multiconfigurational methods. In the future, we hope to validate our approach for a number of real-world applications, such as those involving transition metals and lanthanides, for which many more qubits are required to perform simulations using quantum devices, and we hope to extend our approach to simulations of molecular excited states.

This manuscript is organized as follows: Section 2 describes the methods taken in the proposed approach. Section 3 is the main body of this manuscript. It begins with Section 3.1 demonstrating selection of the active space and validation of the model using a conventional computer. Section 3.2 presents results obtained with the VQE algorithm with the use of the statevector simulator, which simulates the ideal execution of a quantum circuit. Sections 3.3 and 3.4 present the result of VQE on a noisy quantum device, with particular attention paid to improving accuracy with error mitigation techniques. Section 4 concludes the paper.

2. METHODS

The reaction under investigation involves conversion of the lithium superoxide caged dimer reactant into the linear dimer product via a transition structure (TS) containing partially broken bonds in the "bridge" formed by lithium and oxygen atoms as shown in Figure 1. The overall strategy for these investigations involves initial preprocessing with classical quantum chemistry codes on conventional computers to generate optimized geometries and guess orbitals prior to performing computations with quantum devices.

2.1. Geometry Optimizations. Classical calculations were performed with the Jaguar module[28] contained in the Schrödinger software suite,[29] in which initial molecular geometries of the reactant and product from previously published literature sources[17] were used and then optimized with the B3LYP[30−33] method, to which dispersion corrections, as described by Grimme et al.,[34] were applied. The resulting B3LYP-D3 procedure was coupled with the 6-311++G(d,p) basis set.[35,36] An initial guess for the transition structure (TS) connecting the reactant and product dimers was determined using Auto TS,[37] a module of the Schrödinger software package. Because of the flat nature of the potential energy surface (PES) in the region of the TS,[17] an analytic Hessian was used for the TS search and for optimization of the initial-guess geometry. Intrinsic reaction coordinate (IRC) analysis was performed on the optimized geometry of the TS to confirm that it was connected to the reactant and product.

2.2. Selection of Active Orbitals. The procedure that we adopted to select the set of molecular orbitals is as follows: (i) first, the PYSCF[38] package was used to perform CISD and CCSD calculations with the 6-311++G(d,p) basis set on the optimized geometries; (ii) second, based on the dominant configurations of CISD and CCSD results, an active space including all of the important valence orbitals and vacant orbitals was chosen and a Full CI calculation was performed on the reactant, TS, and product; and (iii) finally, orbitals that possessed excitation determinants from CI configurations with coefficients greater than 0.05 were chosen as the active space to perform Full CI calculations on quantum simulator and real device.

Note that this method is useful for current devices possessing a limited number of noisy qubits but is expected to become less practical as the number of qubits required for computation of chemical processes increase beyond the point at which classical computers can perform practical calculations of chemical systems with FCI and closely related methods.[39]

2.3. VQE Calculations. Having selected the set of orbitals belonging to the active space for the stationary points, quantum computations were performed with quantum simulators and devices using VQE.[3] Note that, in contrast with quantum chemistry on conventional computers, in which the molecular spin state needs to be predefined to compute the most stable electronic state, the VQE algorithm automatically minimizes the energy to the most stable spin state because the direction of the spin freely rotates at every qubit.[40] An addendum to this is that an initial state needs to be precomputed via a classical algorithm on a conventional computer. The HF singlet state has been chosen as the initial state for all of the calculations described in this manuscript because previous publications have shown that this is a good choice for an initial state.[41] For consistency with the active spaces that we have chosen for these investigations, the energies of orbitals from the singlet state were also used for the orbitals that remained inactive. Since previous publications have indicated that the triplet surface for the rearrangement of the lithium superoxide dimer is very similar to that of the rearrangement on the singlet surface,[17] the HF singlet state is an appropriate reference state that can be used to estimate the correlation energy to the reaction surface.

The Aqua module contained in Qiskit version 0.12[42] with an interface to PySCF was used for all VQE calculations. The conjugate gradient (CG)[43] method for energy minimization was used for calculations on simulators and the simultaneous perturbation stochastic approximation (SPSA)[44,45] method was used for calculations on quantum devices. The quantum unitary coupled cluster singles and doubles (qUCCSD)[46−48] method and three heuristic variational forms (*Ry*, *RyRz*, and *SwapRz*)[49] were compared. Transformation from the fermionic Hamiltonian into the qubit Hamiltonian was accomplished by the parity mapping scheme for qUCCSD, *Ry*, and *RyRz*, while the Jordan−Wigner transformation,[50] was used for *SwapRz*.

2.4. Experiments on Quantum Devices. The IBM 20-qubit backends, ibmq_almaden and ibmq_johannesburg, (henceforth referred to as device a and device j) were used to perform experiments on quantum devices. A set of two qubits with direct connectivity, small readout error rates, and small two-qubit error rates was chosen for those experiments. The expectation value of each Pauli term in the Hamiltonian was measured using 8192 shots. Since current quantum devices are error-prone, the readout error mitigation technique included in Qiskit was used to improve upon errors incurred during qubit readout. The measurement calibration matrix was updated with every VQE iteration to ensure that experimental conditions during readout measurement calibration and VQE iteration were similar. The final energy values reported for VQE experiments on the hardware are based on the lowest

https://dx.doi.org/10.1021/acs.jpca.0c09530
J. Phys. Chem. A 2021, 125, 1827−1836

moving average over 100 VQE data points, with a moving window of 10 data points. SPSA optimizations were carried out for 300−900 iterations for the reactant, product, and TS (see the Supporting Information for further details).

2.5. Application of Quantum State Tomography. To obtain purified ground states from highly mixed states on noisy near-term quantum devices we have applied quantum state tomography as follows (see Figure S2 for an illustrative flowchart): (i) the energy of the ground state computed by VQE, $|\psi_0\rangle$, is minimized to find the mean energy, $E(\theta) = \langle\psi(\theta)|H|\psi(\theta)\rangle$, where $|\psi(\theta)\rangle$ is a parameterized ansatz state; (ii) when $|\psi(\theta)\rangle$ converges, quantum state tomography is performed on the final VQE results to obtain the corresponding density matrix, ρ_{final}; (iii) next, the dominant eigenstate of ρ_{final}, $|\psi_0\rangle$ was computed by diagonalizing ρ_{final}; and (iv) finally, the converged energy from quantum device is corrected as $\langle\psi_0|H|\psi_0\rangle$.

3. RESULTS AND DISCUSSION

3.1. Calculations with a Conventional Computer. The main aims of precomputations with a classical computer are to perform geometry optimizations, described in Section 2.1, and to determine how to reduce the size of the active space eventually used in VQE calculations in an effort to decrease the computational effort necessary to perform calculations on quantum simulator and devices. To expand on the methods outlined in Section 2.2, Full CI was employed to analyze the most important determinants of stationary points that utilize an active space ranging from highest occupied molecular orbital (HOMO)-7 to lowest unoccupied molecular orbital (LUMO)-7. This analysis uncovered the most important contributions to electron correlation comprise two orbitals (HOMO and LUMO) for the reactant and two orbitals (HOMO-6 and LUMO) for both transition structure and product (Figure 2). The energies of the reactant, TS, and

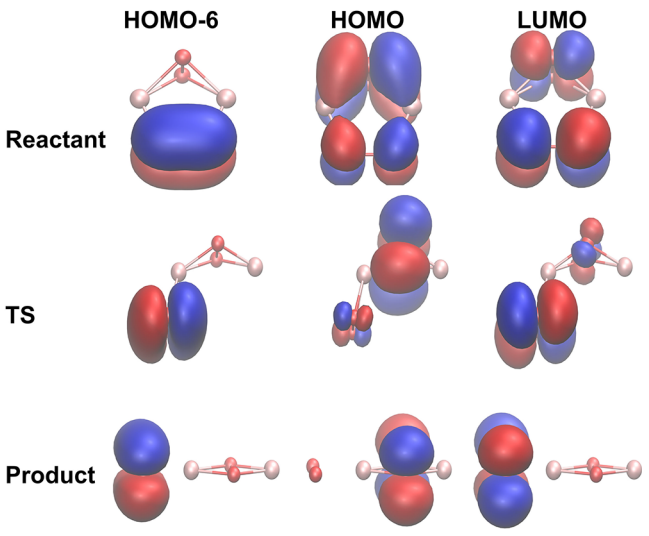

Figure 2. Active orbitals and energies (in Ha) from HF calculations.

product were obtained with HF and with FCI using two sets of reduced active spaces (HOMO/LUMO and HOMO-6/HOMO/LUMO) and are shown in Table 1; the accompanying energy profile is shown in Figure 3. HF predicts that the energy of the reactant is much higher than the TS and product suggesting that the reaction mechanism possesses no barrier, presumably due to the fact that electron correlation is missing. In contrast, FCI, which accounts for electron correlation, predicts that the energy of the reactant is more stable than that of the TS and the energetic barriers are predicted to be 78 and 21 mHa with the HOMO/LUMO and HOMO-6/HOMO/LUMO active spaces, respectively. Comparison of these results with those utilizing a much larger active space comprising the HOMO-7 to LUMO-7 orbitals indicates that orbitals involving the HOMO-6/HOMO/LUMO provide a reasonable description of the reaction pathway.

The biradical character of the reactant, TS, and product was examined by comparing the ground and first excited states (GS and ES_1) using FCI. As shown in Figure 4, the energy difference for the reactant is only 0.7 mHa but increases to 135.8 mHa as the reaction proceeds from reactant to product. This implies that the biradical character for the reactant is strong while the TS and product exhibit little biradical character. This fact requires that the spin configuration of the reactant needs to be described by correlated methods that can accurately describe the superposition of the singlet and triplet states.

3.2. Calculations with the Statevector Simulator. With geometries and energies from classical computation in hand, we then turned to computations with a quantum simulator to determine energies and reaction profiles for the HOMO/LUMO and HOMO-6/HOMO/LUMO active spaces of these stationary points. Figures 5 and 6 show comparisons of energies of the reactant, TS, and product computed with qUCCSD and heuristic ansatze (*Ry*, *RyRz*, and *SwapRz*) with the exact eigensolver using the 6-311++G(d,p) basis set. These results demonstrate that qUCCSD and all of the heuristic ansatze predict energies similar to the exact eigensolver when the HOMO/LUMO active space is used. On the other hand, for the active space comprising HOMO-6/HOMO/LUMO, although the qUCCSD wavefunction can reproduce the exact values at circuit depth = 1, a circuit depth = 3 is required to match exact values when heuristic trial ansatze are used. These results indicate that the circuit depth required by heuristic methods may increase when the number of active orbitals are increased. We note that the reason the qUCCSD ansatz reproduces FCI is due to the fact only the singles and doubles excitation contributes to the electron correlation in the system under test.[51]

The number of CNOT gates in the circuit and the number of optimization parameters (OptParams) used in the VQE algorithm for all of the heuristic methods have been compared in Table 2 to determine which ansatz would be suitable for use on the real device for a two-qubit system. As these results show, when circuit depth = 1, circuits involving the use of qUCCSD and *SwapRz* ansatze possess four CNOT gates, whereas only one CNOT gate is required for the *Ry* and *RyRz* ansatze. Note that *SwapRz* requires four qubits for an active space with two molecular orbitals, whereas all of the other ansatze require two qubits after applying two-qubit reduction by parity.

Moreover, increasing the depth to 2 results in the addition of four CNOT gates when the qUCCSD and *SwapRz* ansatze are used, but a similar increase in the depth only increases the number of CNOT gates required for the *Ry* and *RyRz* ansatze by a single gate. Similarly, the number of optimization parameters required for VQE calculations linearly increases in the order qUCCSD < *Ry* < *SwapRz* < *RyRz* for circuit depth equaling 1, but at higher circuit depths the order for the

https://dx.doi.org/10.1021/acs.jpca.0c09530
J. Phys. Chem. A 2021, 125, 1827−1836

Table 1. HF and FCI Energies, in Ha, of the Reactant, TS, and Product Computed with the 6-311++G(d,p) Basis Set Various Active Spaces. Energies (in mHa) Relative to Reactants Are Shown in Parentheses[aa]

	HF	FCI (2 orbitals)	FCI (3 orbitals)	FCI (16 orbitals)
reactant	−314.153739 (0)	−314.270197 (0)	−314.270893 (0)	−314.271560 (0)
TS	−314.189526 (−36)	−314.192609 (78)	−314.249585 (21)	314.252918 (19)
product	−314.212670 (−59)	−314.212670 (58)	−314.271925 (−1)	−314.274153 (−3)

[a]1 Ha = 627.5095 kcal/mol.

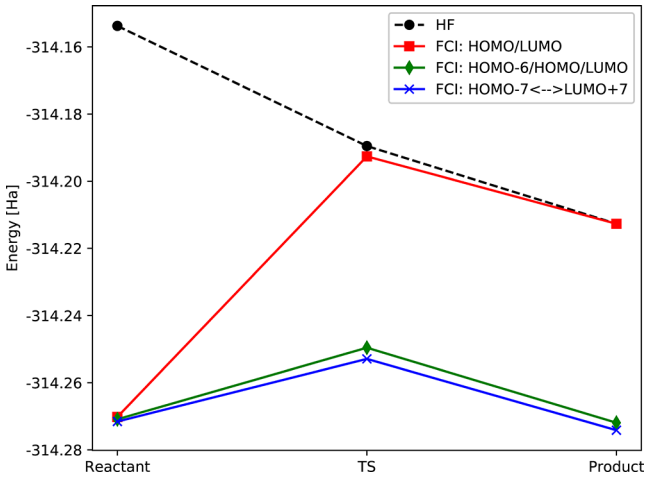

Figure 3. Active orbitals and energies (in Ha) from HF calculations.

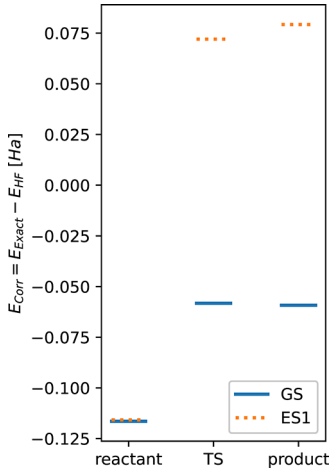

Figure 4. Energies of the ground and first excited states (GS and ES_1, respectively) for reactant, TS, and product (1 Ha = 627.5095 kcal/mol).

increase in the number of optimization parameters changes to *Ry* < qUCCSD ≈ *SwapRz* < *RyRz*.

To obtain reliable results from a quantum device in a reasonably short time, an ansatz with few CNOT gates and few optimization parameters is needed, since the CNOT error rate influences the accuracy of the computed results and the number of optimization parameters is proportional to the number of iterations required for energy convergence. Accordingly, because *Ry* possesses comparatively fewer CNOT gates and optimization parameters than the other ansatze even with higher circuit depths, it was selected as the most suitable ideal choice of those available for calculations on the quantum device.

3.3. Calculations on Quantum Devices. To describe all of the electronic arrangement that will occur during the lithium

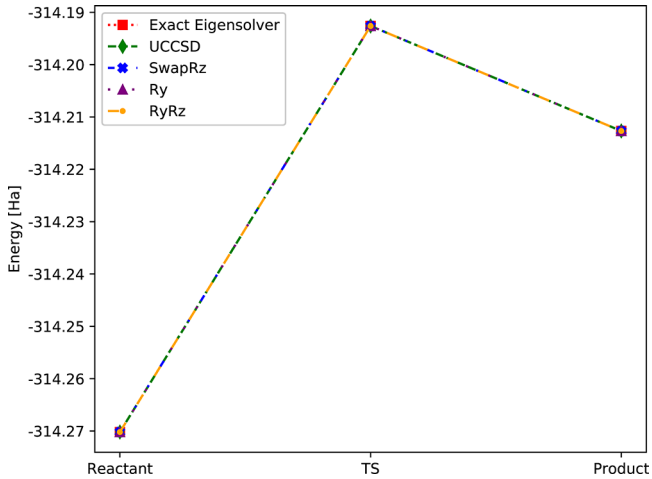

Figure 5. Energies of reactant, transition state, and product as computed by the (a) qUCCSD, (b) *SwapRz*, (c) *Ry*, and (d) *RyRz* ansatze. The HOMO and LUMO were used as the active space for all calculations (1 Ha = 627.5095 kcal/mol).

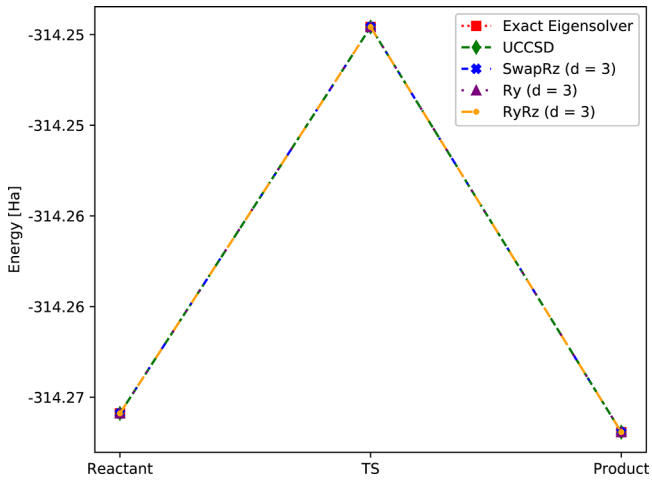

Figure 6. Energies of reactant, transition state, and product as computed by the (a) qUCCSD, (b) *SwapRz*, (c) *Ry*, and (d) *RyRz* ansatze. The HOMO-6, HOMO, and LUMO were used as the active space for all calculations (1 Ha = 627.5095 kcal/mol).

superoxide dimer rearrangement process, an active space comprising HOMO-6/HOMO/LUMO is required based on the results shown in Figure 3. To perform the calculations on the quantum device, we further truncate these orbitals to HOMO and LUMO for reactant and HOMO-6 and LUMO for the TS and product. The truncation of HOMO-6/HOMO/LUMO to HOMO/LUMO for reactant and HOMO-6/LUMO for TS and product is based on results obtained with a conventional computer, which indicate that the resulting wavefunction with active space of HOMO-6/HOMO/LUMO for the reactant is mainly composed of fractional contributions

https://dx.doi.org/10.1021/acs.jpca.0c09530
J. Phys. Chem. A 2021, 125, 1827−1836

Table 2. Number of CNOT Gates and Optimization Parameters (OptParams) Required at Circuit Depths, *d*, Ranging from 1 to 3 with the qUCCSD, *SwapRz*, *Ry*, and *RyRz* Ansatze with Two Qubits

	CNOT gates			OptParams		
	$d = 1$	$d = 2$	$d = 3$	$d = 1$	$d = 2$	$d = 3$
qUCCSD	4	8	12	3	6	9
SwapRz	4	8	12	5	8	11
Ry	1	2	3	4	6	8
RyRz	1	2	3	8	12	16

from the HOMO and LUMO. Similarly, the occupations are mainly derived from orbitals HOMO-6 and LUMO for the TS and product. Consequently, the linear expansion of multiple of electronic configurations using active space of HOMO/LUMO for reactant and HOMO-6/LUMO for TS and product should be similar to those using active space of HOMO-6/HOMO/LUMO. Such truncation helps us to reduce the computational cost of accurate calculations, which is a practical issue for the current noisy quantum device. This choice of active space with two spatial orbitals corresponds to a two-qubit system after applying two-qubit reduction provided by the use of parity mapping. Furthermore, based on results obtained from the quantum simulator experiments, the *Ry* ansatz with circuit depth = 1 was used in combination with readout error mitigation (which dominates the offset to the exact energy and its fluctuation for these shallow circuits) on raw measurement counts on quantum devices to reduce the measurement error.

Figure 7a–c shows trends in energy minimization for the reactant, TS, and product, respectively, as a function of readout error-mitigated VQE calculations on device a and device j. Figure 7d summarizes the results in Table 3 with energies of stationary points relative to the reactant. As shown, calculations performed on both devices exhibit different trends, but both are competent at almost reproducing the energies obtained with Full CI. The energy of the product predicted by calculations involving device a underestimates the Full CI energy by 1 mHa, but the TS energy is overestimated by 3 mHa. In contrast, device j predicts energies for the TS and product that are nearly the same as those predicted by Full CI. As for the reactant, both devices underestimate the exact energies by ∼5 mHa. As a consequence, simulations on device a underestimates the reaction barrier by 8 mHa and overestimates the reaction energy by 3 mHa with respect to the energy of the reactant. Similarly, simulations on device j device underestimates the barrier and overestimates the reaction energy by 5 mHa in both cases. The good performance in predicting the exact energies is attributed to the careful choice of ansatz (use of the *Ry* circuit with two qubits), the choice of the classical optimizer (SPSA, which is well suited to the stochasticity of the quantum device) and the application of readout error mitigation.

Although energies obtained by quantum computation using the readout error-mitigated VQE algorithm are nearly equal to the exact energies of stationary points on the potential energy surface, we emphasize that this does not necessarily mean that the ansatz state converges to the target ground state. Convergence can be evaluated by computing the overlap (fidelity) of those two states during the VQE process, which is the absolute value of the inner product of the target ground state and the ideal ansatz state with the parameters obtained from the experiment. The overlap, *S*, is given by eq 1

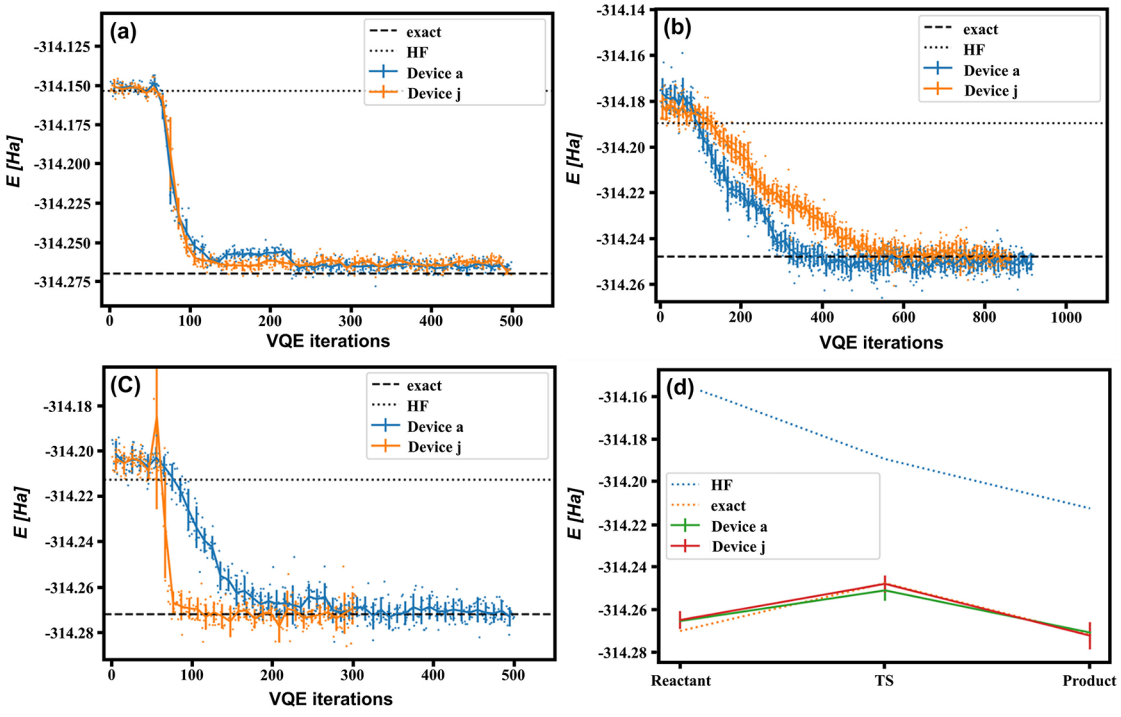

Figure 7. VQE iterations for calculations on device a and device j quantum devices for the HOMO/LUMO active space of (a) the reactant and the HOMO-6/LUMO active spaces of (b) the TS and (c) product of the lithium superoxide caged dimer. (d) Summary of the results obtained for the three structures with HF, the exact eigensolver, and VQE on the readout error-mitigated hardware experiments using the *Ry* ansatz with circuit depth = 1 (1 Ha = 627.5095 kcal/mol).

https://dx.doi.org/10.1021/acs.jpca.0c09530
J. Phys. Chem. A 2021, 125, 1827–1836

Table 3. Comparison of Energies (in Ha) Computed Using the HOMO/LUMO Active Space for Reactant, and the HOMO-6/LUMO Active Space for the Transition State and Product with the Exact Eigensolver and the *Ry* Heuristic Ansatz on the Statevector Simulator and on Device a and Device j Using the *Ry* Ansatz at Circuit Depth = 1 with Readout Error Mitigation[a]

	reactant	TS	product
HF	−314.153739 (0)	−314.189526 (−36)	−314.212670 (−59)
Ry, statevector simulator	−314.270196 (0)	−314.247749 (22)	−314.271916 (−2)
Ry, device a with readout error mitigation	−314.277634 ± 0.003764 (0)	−314.245832 ± 0.0051806 (32)	−314.267923± 0.006123 (10)
Ry, device j with readout error mitigation	−314.267807 ± 0.008554 (0)	−314.242478 ± 0.006081 (25)	−314.2757615 ± 0.007002 (−8)
exact	−314.270196 (0)	−314.247750 (22)	−314.271916 (−2)

[a]Energies relative to reactants (in mHa) are shown in parentheses. 1 mHa = 0.6275095 kcal/mol.

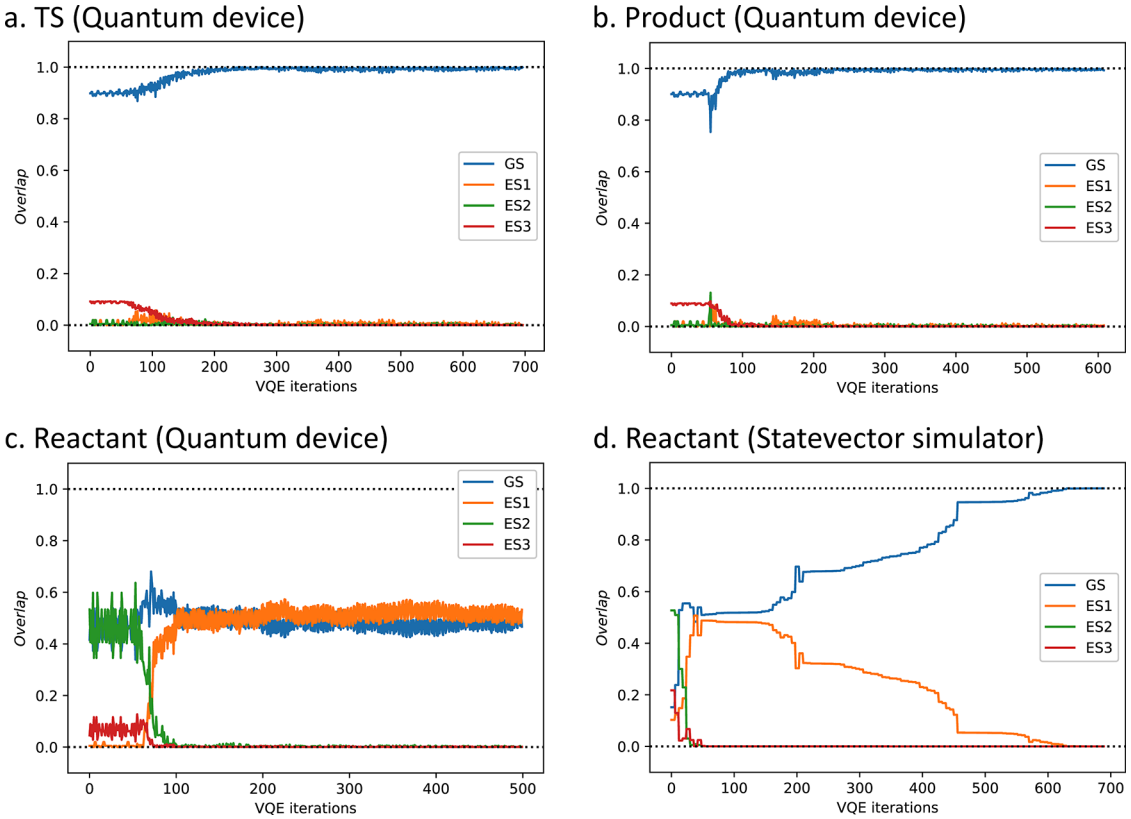

Figure 8. Overlap (S_k^j) between the VQE state and the expected eigenstates of the stationary points as a function of VQE iterations (optimizer steps), k, on quantum hardware for (a) the TS (HOMO-6 and LUMO active space), $S_{\text{VQE-TS}} = 1$; (b) the product (HOMO-6 and LUMO active space), $S_{\text{VQE-product}} = 1$; (c) the reactant (HOMO−LUMO active space) $S_{\text{VQE-reactant}} \approx 0.55$ (HOMO−LUMO active space); and (d) the statevector simulator $S_{\text{VQE-reactant}} = 1$.

$$S_k^j = |\langle \psi^j | \psi(\theta^{(k)}) \rangle|^2 \tag{1}$$

where $|\psi^j\rangle$ is the jth eigenstate of the Hamiltonian and $|\psi(\theta^{(k)})\rangle$ is the VQE state at the kth iteration of the optimization process. We observe that the overlap converges to the optimal value of 1 for the TS and product (see Figure 8a,b for details), indicating that this is the pure ground state. However, in the case of the reactant, the overlap converges to ∼0.55 as shown in Figure 8c. This signifies that the resulting state generated by VQE is not the pure ground state. Note that, in contrast, simulation without noise succeeds in finding the ground state of the reactant as shown in Figure 8d.

3.4. Error Improvement by Quantum State Tomography. To further mitigate this error, previous protocols have employed the Richardson extrapolation method,[5] and symmetry-adapted methods have also been proposed for ansatze[52] and postselection[53] routines. Here, we propose an alternative method based on the use of quantum state tomography method in which the quantum state of the qubits prepared by the ansatz in a density matrix is reconstructed. A similar approach has recently been developed.[54]

First, performing state tomography on the final VQE step produces a density matrix (shown in eq 2 is obtained by performing state tomography on the final VQE step.

$$\rho_{\text{final}} = \begin{bmatrix} 0.539 & 0.320 - 0.002i & -0.237 + 0.021i & -0.180 - 0.011i \\ 0.320 + 0.002i & 0.212 & -0.135 + 0.015i & -0.109 - 0.006i \\ -0.237 - 0.021i & -0.135 - 0.015i & 0.159 & 0.116 + 0.022i \\ -0.180 + 0.011i & -0.109 + 0.006i & 0.116 - 0.022i & 0.090 \end{bmatrix} \tag{2}$$

The target space is spanned by four determinants $\{\phi_{H\uparrow}\phi_{L\downarrow}, \phi_{H\uparrow}\phi_{H\downarrow}, \phi_{L\uparrow}\phi_{L\downarrow}, \phi_{H\downarrow}\phi_{L\uparrow}\}$ described with occupied spin HOMO, ϕ_H, and spin LUMO, ϕ_L, with up or down spin, in accordance with the two-orbital and two-electron complete active space (CAS).

https://dx.doi.org/10.1021/acs.jpca.0c09530
J. Phys. Chem. A 2021, 125, 1827−1836

Next, this density matrix can be diagonalized to determine the eigenstates as shown in eq 3.

$$\rho_{\text{final}} = \sum_i \lambda_i |\psi_i\rangle\langle\psi_i| \tag{3}$$

The dominant eigenstate $|\psi_0\rangle$ has the largest eigenvalue, ψ_0 = 0.914. Finally, the energy calculated at the final VQE step is corrected as shown in eq 4.

$$E = \langle\psi_0|H|\psi_0\rangle \tag{4}$$

In general, the computational cost for performing state tomography of an n qubit system scales as 4^n. To reduce the cost, a computationally inexpensive iterative method[55] with the Lánczos method[56] can be used instead of direct diagonalization. However, while this method is useful for mean-field or one-electron calculations, it is not applicable in the case of systems comprising biradical species. Moreover, while the use of the Lánczos method can only reduce the computational cost to 2^n, it is still limited to calculations that can be performed on near-term devices with limited qubits. Much more efficient methods would be required for state tomography for calculations performed on larger quantum devices, for which we note that there has been some recent progress.[57,58]

Error mitigation of VQE results by state tomography are compared with that obtained using only readout error mitigation in Figure 9. Without error mitigation, VQE predicts

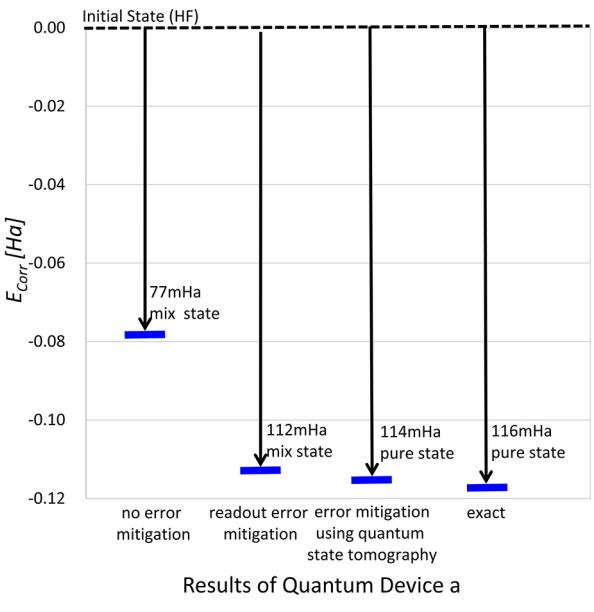

Figure 9. Correlation energies of the reactant computed by the *Ry* ansatz using VQE on device a with and without error mitigation.

that the correlation energy obtained from *Ry* is about −77 mHa. This differs from the correlation energy of the exact value (−116 mHa) by 39 mHa, which is the net noise volume. Readout error correction applied to the *Ry* result successfully reduces the correlation energy to −112 mHa at steady state. This signifies that the readout noise is about 35 mHa, from which 4 mHa (with respect to the net noise volume) stems from noise due to quantum decoherence. The use of state tomography reduces the deviation to within 2 mHa of the exact value, indicating mitigation of not only the readout error but also the process error.

We surmise that VQE cannot determine a pure ground state of the reactant is that the energy gap between the ground and first excited states, δ_{reac}, is 0.000698, which is much smaller than the measurement standard deviation, $\sqrt{(\Delta H^2_{\text{reac}})}$ = 0.131976; thus, $|\text{GS}\rangle$ and $|\text{ES}_1\rangle$ cannot be distinguished. To correctly obtain the GS of the reactant, the error must be suppressed enough that the condition $\delta_{\text{reac}} \gtrsim \sqrt{(\Delta H^2_{\text{reac}})}$ is satisfied, although it is not feasible to achieve such a small measurement error in practice. Notably, $|\psi_0\rangle$ is approximated by the superposition of the ground and first excited states by projecting to the eigenstates of the Hamiltonian, as shown in eq 5. This is in agreement with the overlap between the VQE state and expected eigenstates shown in Figure 8c.

$$|\psi_0\rangle \approx 0.672|\text{GS}\rangle - 0.727|\text{ES}_1\rangle \tag{5}$$

Equation 5 indicates that for these strongly biradical molecules in which the GS and ES_1 are nearly degenerate, VQE converges to the spuriously mixed state. To remove this spin contamination, we introduce a postprocessing method in which the previous eigendecomposition is performed on the density matrix with the disjointed singlet and triplet subspaces. This protocol is described in Section 2.5 and the Supporting Information.

For the specific case of the reactant investigated in this manuscript, the density matrix has been transformed from the determinantal basis to the spin-adapted basis, couplings between the eigen-subspaces of the spin multiplicity have been removed, and each subspace has been diagonalized (see the Supporting Information for details). Indeed, this approach leads to the faithful reproduction of the purified GS eigenvector in which VQE energy exhibits no mixing presumably due to the lack of correlation among different spin multiplicities in the Hamiltonian. Thus, it appears that such subspace decoupling could potentially be a useful postprocessing option to contend with spin contamination arising from VQE calculations on nearly degenerate biradicals and other polyradicals on near-term quantum devices.

4. CONCLUSIONS

In summation, the VQE algorithm has been used to investigate the rearrangement of the lithium superoxide dimer from its caged structure into its linear analogue with a variety of ansatze on a quantum simulator and on current hardware. Calculations performed with a quantum simulator reproduced exact values. Calculations performed using the ibmq_almaden and ibmq_johannesburg quantum devices were capable of generating results that were within a few millihartrees of exact values for structures on the potential energy surfaces for the rearrangement. This achievement is attributed to precomputation on classical hardware, which helped us to identify reduced active spaces, comprising the HOMO/LUMO and HOMO-6/HOMO/LUMO orbitals, that are appropriate choices for the quantum simulation of this chemical process and served to reduce the number of qubits required for quantum computation.

We have found that the VQE algorithm is challenged to accurately simulate biradical species on a noisy present-day quantum device due to the influence of device noise. We have investigated the use of an error mitigation approach using the state tomography technique to improve the accuracy of VQE simulations on quantum devices. We have shown that quantum

https://dx.doi.org/10.1021/acs.jpca.0c09530
J. Phys. Chem. A 2021, 125, 1827−1836

state tomography could identify that the quantum state of the reactant investigated in this study, which has a strong biradical character, converged to a state, which is a superposition of the GS and ES_1 spin states. Moreover, using a spin-projected unitary operator of the density matrix obtained from VQE calculations, this approach can be effectively used to remove the ES_1 spin state. In the future, we hope to validate our approach for a number of real-world applications, such as those involving transition metals and lanthanides, for which many more qubits are required to perform simulations using quantum devices, and we hope to extend our approach to simulations of molecular excited states.

■ ASSOCIATED CONTENT

Supporting Information

The Supporting Information is available free of charge at https://pubs.acs.org/doi/10.1021/acs.jpca.0c09530.

Tables of energies computed with various active spaces; Cartesian coordinates of stationary points; and descriptions of how mean and standard deviations for VQE energies were computed on quantum devices (PDF)

■ AUTHOR INFORMATION

Corresponding Authors

Qi Gao − *Mitsubishi Chemical Corporation Science & Innovation Center, Yokohama 227-8502, Japan; Quantum Computing Center, Keio University, Yokohama 223-8522, Japan*; Email: caoch@user.keio.ac.jp

Jeannette M. Garcia − *IBM Quantum, IBM Research−Almaden, San Jose, California 95120, United States*; orcid.org/0000-0002-8336-4592; Email: jmgarcia@us.ibm.com

Naoki Yamamoto − *Quantum Computing Center, Keio University, Yokohama 223-8522, Japan*; Email: yamamoto@appi.keio.ac.jp

Authors

Hajime Nakamura − *Quantum Computing Center, Keio University, Yokohama 223-8522, Japan; IBM Quantum, IBM Research−Tokyo, Tokyo 103-8510, Japan*

Tanvi P. Gujarati − *IBM Quantum, IBM Research−Almaden, San Jose, California 95120, United States*

Gavin O. Jones − *IBM Quantum, IBM Research−Almaden, San Jose, California 95120, United States*; orcid.org/0000-0003-1528-6438

Julia E. Rice − *IBM Quantum, IBM Research−Almaden, San Jose, California 95120, United States*

Stephen P. Wood − *IBM Thomas J. Watson Research Center, Yorktown Heights, New York 10598, United States*

Marco Pistoia − *IBM Thomas J. Watson Research Center, Yorktown Heights, New York 10598, United States*

Complete contact information is available at: https://pubs.acs.org/10.1021/acs.jpca.0c09530

Author Contributions

Q.G. conceived the idea of this work and performed calculations on classical computers and on quantum simulators. H.N. and T.P.G. performed experiments on quantum devices. J.E.R. and Q.G. performed active space analyses with the FCI method. S.P.W. and M.P. contributed developments to the Qiskit software that enabled enhanced computational features. N.Y. performed quantum state tomography analyses. Q.G. and J.M.G. supervised the work. G.O.J. wrote the manuscript, and all authors contributed to the continuous improvement of the manuscript.

Notes

The authors declare no competing financial interest.

■ ACKNOWLEDGMENTS

Q.G., H.N., and N.Y. acknowledge support from MEXT Quantum Leap Flagship Program Grant No. JPMXS0118067285. Q.G. thanks Dr. Takao Kobayashi from the Mitsubishi Chemical Corporation Science & Innovation Center for discussions on selecting an appropriate active space.

■ REFERENCES

(1) Preskill, J. Quantum Computing in the NISQ Era and Beyond. *Quantum* **2018**, *2*, No. 79.

(2) Kitaev, A. Y. Quantum Measurements and the Abelian Stabilizer Problem. 1995, arXiv:quant-ph/9511026. arXiv.org e-Print archive. https://arxiv.org/abs/quant-ph/9511026.

(3) Peruzzo, A.; McClean, J.; Shadbolt, P.; Yung, M.-H.; Zhou, X.-Q.; Love, P. J.; Aspuru-Guzik, A.; O'Brien, J. L. A Variational Eigenvalue Solver on a Photonic Quantum Processor. *Nat. Commun.* **2014**, *5*, No. 4213.

(4) Kandala, A.; Mezzacapo, A.; Temme, K.; Takita, M.; Brink, M.; Chow, J. M.; Gambetta, J. M. Hardware-Efficient Variational Quantum Eigensolver for Small Molecules and Quantum Magnets. *Nature* **2017**, *549*, 242−246.

(5) Kandala, A.; Temme, K.; Córcoles, A. D.; Mezzacapo, A.; Chow, J. M.; Gambetta, J. M. Error Mitigation Extends the Computational Reach of a Noisy Quantum Processor. *Nature* **2019**, *567*, 491−495.

(6) Ollitrault, P. J.; Kandala, A.; Chen, C.-F.; Barkoutsos, P. K.; Mezzacapo, A.; Pistoia, M.; Sheldon, S.; Woerner, S.; Gambetta, J.; Tavernelli, I. Quantum Equation of Motion for Computing Molecular Excitation Energies on a Noisy Quantum Processor. *Phys. Rev. Res.* **2020**, *2*, No. 043140.

(7) Anslyn, E. V.; Dougherty, D. A. *Modern Physical Organic Chemistry*; University Science Books, 2006.

(8) Moss, R. A.; Platz, M. S.; Jones, M., Jr. *Reactive Intermediate Chemistry*; Wiley, 2003.

(9) McCaskey, A. J.; Parks, Z. P.; Jakowski, J.; Moore, S. V.; Morris, T. D.; Humble, T. S.; Pooser, R. C. Quantum Chemistry as a Benchmark for Near-Term Quantum Computers. *npj Quantum Inf.* **2019**, *5*, No. 99.

(10) Ibe, Y.; Nakagawa, Y. O.; Yamamoto, T.; Mitarai, K.; Gao, Q.; Kobayashi, T. Calculating Transition Amplitudes by Variational Quantum Eigensolvers. 2020, arXiv:2002.11724. arXiv.org e-Print archive. https://arxiv.org/abs/2002.11724.

(11) Aurbach, D.; McCloskey, B. D.; Nazar, L. F.; Bruce, P. G. Advances in Understanding Mechanisms Underpinning Lithium−Air Batteries. *Nat. Energy* **2016**, *1*, No. 16128.

(12) Imanishi, N.; Luntz, A. C.; Bruce, P. *The Lithium Air Battery: Fundamentals*; Springer-Verlag, New York, 2014.

(13) Grande, L.; Paillard, E.; Hassoun, J.; Park, J.-B.; Lee, Y.-J.; Sun, Y.-K.; Passerini, S.; Scrosati, B. The Lithium/Air Battery: Still an Emerging System or a Practical Reality? *Adv. Mater.* **2015**, *27*, 784−800.

(14) Abraham, K. M. Prospects and Limits of Energy Storage in Batteries. *J. Phys. Chem. Lett.* **2015**, *6*, 830−844.

(15) Lu, J.; Li, L.; Park, J.-B.; Sun, Y.-K.; Wu, F.; Amine, K. Aprotic and Aqueous $Li-O_2$ Batteries. *Chem. Rev.* **2014**, *114*, 5611−5640.

(16) Mahne, N.; Fontaine, O.; Thotiyl, M. O.; Wilkening, M.; Freunberger, S. A. Mechanism and Performance of Lithium−Oxygen Batteries − a Perspective. *Chem. Sci.* **2017**, *8*, 6716−6729.

(17) Bryantsev, V. S.; Blanco, M.; Faglioni, F. Stability of Lithium Superoxide LiO_2 in the Gas Phase: Computational Study of Dimerization and Disproportionation Reactions. *J. Phys. Chem. A* **2010**, *114*, 8165−8169.

(18) Das, U.; Lau, K. C.; Redfern, P. C.; Curtiss, L. A. Structure and Stability of Lithium Superoxide Clusters and Relevance to Li−O_2 Batteries. *J. Phys. Chem. Lett.* **2014**, *5*, 813−819.
(19) Ditchfield, R.; Hehre, W. J.; Pople, J. A. Self-Consistent Molecular-Orbital Methods. IX. An Extended Gaussian-Type Basis for Molecular-Orbital Studies of Organic Molecules. *J. Chem. Phys.* **1971**, *54*, 724−728.
(20) Hariharan, P. C.; Pople, J. A. The Influence of Polarization Functions on Molecular Orbital Hydrogenation Energies. *Theor. Chim. Acta* **1973**, *28*, 213−222.
(21) Hariharan, P. C.; Pople, J. A. Accuracy of AH n Equilibrium Geometries by Single Determinant Molecular Orbital Theory. *Mol. Phys.* **1974**, *27*, 209−214.
(22) Francl, M. M.; Pietro, W. J.; Hehre, W. J.; Binkley, J. S.; Gordon, M. S.; DeFrees, D. J.; Pople, J. A. Self-consistent Molecular Orbital Methods. XXIII. A Polarization-type Basis Set for Second-row Elements. *J. Chem. Phys.* **1982**, *77*, 3654−3665.
(23) Gordon, M. S. The Isomers of Silacyclopropane. *Chem. Phys. Lett.* **1980**, *76*, 163−168.
(24) Binning, R. C.; Curtiss, L. A. Compact Contracted Basis Sets for Third-Row Atoms: Ga−Kr. *J. Comput. Chem.* **1990**, *11*, 1206−1216.
(25) Blaudeau, J.-P.; McGrath, M. P.; Curtiss, L. A.; Radom, L. Extension of Gaussian-2 (G2) Theory to Molecules Containing Third-Row Atoms K and Ca. *J. Chem. Phys.* **1997**, *107*, 5016−5021.
(26) Rassolov, V. A.; Pople, J. A.; Ratner, M. A.; Windus, T. L. 6-31G* Basis Set for Atoms K through Zn. *J. Chem. Phys.* **1998**, *109*, 1223−1229.
(27) Clark, T.; Chandrasekhar, J.; Spitznagel, G. W.; Schleyer, P. V. R. Efficient Diffuse Function-Augmented Basis Sets for Anion Calculations. III. The 3-21+G Basis Set for First-Row Elements, Li−F. *J. Comput. Chem.* **1983**, *4*, 294−301.
(28) Bochevarov, A. D.; Harder, E.; Hughes, T. F.; Greenwood, J. R.; Braden, D. A.; Philipp, D. M.; Rinaldo, D.; Halls, M. D.; Zhang, J.; Friesner, R. A. Jaguar: A High-Performance Quantum Chemistry Software Program with Strengths in Life and Materials Sciences. *Int. J. Quantum Chem.* **2013**, *113*, 2110−2142.
(29) *Materials Science Suite 2018-3*. Schrödinger, LLC, New York, 2019.
(30) Becke, A. D. Density-functional Thermochemistry. III. The Role of Exact Exchange. *J. Chem. Phys.* **1993**, *98*, 5648−5652.
(31) Lee, C.; Yang, W.; Parr, R. G. Development of the Colle-Salvetti Correlation-Energy Formula into a Functional of the Electron Density. *Phys. Rev. B* **1988**, *37*, 785−789.
(32) Vosko, S. H.; Wilk, L.; Nusair, M. Accurate Spin-Dependent Electron Liquid Correlation Energies for Local Spin Density Calculations: A Critical Analysis. *Can. J. Phys.* **1980**, *58*, 1200−1211.
(33) Stephens, P. J.; Devlin, F. J.; Chabalowski, C. F.; Frisch, M. J. Ab Initio Calculation of Vibrational Absorption and Circular Dichroism Spectra Using Density Functional Force Fields. *J. Phys. Chem. A* **1994**, *98*, 11623−11627.
(34) Grimme, S.; Antony, J.; Ehrlich, S.; Krieg, H. A Consistent and Accurate Ab Initio Parametrization of Density Functional Dispersion Correction (DFT-D) for the 94 Elements H-Pu. *J. Chem. Phys.* **2010**, *132*, 154104−154119.
(35) McLean, A. D.; Chandler, G. S. Contracted Gaussian Basis Sets for Molecular Calculations. I. Second Row Atoms, Z=11−18. *J. Chem. Phys.* **1980**, *72*, 5639−5648.
(36) Krishnan, R.; Binkley, J. S.; Seeger, R.; Pople, J. A. Self-consistent Molecular Orbital Methods. XX. A Basis Set for Correlated Wave Functions. *J. Chem. Phys.* **1980**, *72*, 650−654.
(37) Jacobson, L. D.; Bochevarov, A. D.; Watson, M. A.; Hughes, T. F.; Rinaldo, D.; Ehrlich, S.; Steinbrecher, T. B.; Vaitheeswaran, S.; Philipp, D. M.; Halls, M. D.; et al. Automated Transition State Search and Its Application to Diverse Types of Organic Reactions. *J. Chem. Theory Comput.* **2017**, *13*, 5780−5797.
(38) Sun, Q.; Berkelbach, T. C.; Blunt, N. S.; Booth, G. H.; Guo, S.; Li, Z.; Liu, J.; McClain, J. D.; Sayfutyarova, E. R.; Sharma, S.; et al. PySCF: The Python-Based Simulations of Chemistry Framework. *Wiley Interdiscip. Rev.: Comput. Mol. Sci.* **2018**, *8*, No. e1340.
(39) Vogiatzis, K. D.; Ma, D.; Olsen, J.; Gagliardi, L.; de Jong, W. Pushing Configuration-Interaction to the Limit: Towards Massively Parallel MCSCF Calculations. *J. Chem. Phys.* **2017**, *147*, No. 184111.
(40) Ryabinkin, I. G.; Genin, S. N.; Izmaylov, A. F. Constrained Variational Quantum Eigensolver: Quantum Computer Search Engine in the Fock Space. *J. Chem. Theory Comput.* **2019**, *15*, 249−255.
(41) Romero, J.; Babbush, R.; McClean, J. R.; Hempel, C.; Love, P. J.; Aspuru-Guzik, A. Strategies for Quantum Computing Molecular Energies Using the Unitary Coupled Cluster Ansatz. *Quantum Sci. Technol.* **2019**, *4*, No. 014008.
(42) Aleksandrowicz, G.; Alexander, T.; Barkoutsos, P.; Bello, L.; Ben-Haim, Y.; Bucher, D.; Cabrera-Hernández, F. J.; Carballo-Franquis, J.; Chen, A.; Chen, C.-F. et al. *Qiskit: An Open-Source Framework for Quantum Computing*, Zenodo, 2019.
(43) Hestenes, M. R.; Stiefel, E. Methods of Conjugate Gradients for Solving Linear Systems. *J. Res. Natl. Bur. Stand.* **1952**, *49*, 409−436.
(44) Spall, J. C. An Overview of the Simultaneous Perturbation Method for Efficient Optimization. *Johns Hopkins APL Tech. Dig.* **1998**, *19*, 482−492.
(45) Spall, J. C. Adaptive Stochastic Approximation by the Simultaneous Perturbation Method. *IEEE Trans. Autom. Control* **2000**, *45*, 1839−1853.
(46) Kutzelnigg, W. Quantum Chemistry in Fock Space. I. The Universal Wave and Energy Operators. *J. Chem. Phys.* **1982**, *77*, 3081−3097.
(47) Kutzelnigg, W.; Koch, S. Quantum Chemistry in Fock Space. II. Effective Hamiltonians in Fock Space. *J. Chem. Phys.* **1983**, *79*, 4315−4335.
(48) Kutzelnigg, W. Quantum Chemistry in Fock Space. IV. The Treatment of Permutational Symmetry. Spin-free Diagrams with Symmetrized Vertices. *J. Chem. Phys.* **1985**, *82*, 4166−4186.
(49) Barkoutsos, P. K.; Gonthier, J. F.; Sokolov, I.; Moll, N.; Salis, G.; Fuhrer, A.; Ganzhorn, M.; Egger, D. J.; Troyer, M.; Mezzacapo, A.; et al. Quantum Algorithms for Electronic Structure Calculations: Particle-Hole Hamiltonian and Optimized Wave-Function Expansions. *Phys. Rev. A* **2018**, *98*, No. 022322.
(50) Jordan, P.; Wigner, E. Über das Paulische Äquivalenzverbot. *Z. Phys.* **1928**, *47*, 631−651.
(51) Kühn, M.; Zanker, S.; Deglmann, P.; Marthaler, M.; Weiß, H. Accuracy and Resource Estimations for Quantum Chemistry on a Near-Term Quantum Computer. *J. Chem. Theory Comput.* **2019**, *15*, 4764−4780.
(52) McArdle, S.; Jones, T.; Endo, S.; Li, Y.; Benjamin, S.; Yuan, X. Variational Ansatz-Based Quantum Simulation of Imaginary Time Evolution. *npj Quantum Inf.* **2019**, *5*, No. 75.
(53) Bonet-Monroig, X.; Sagastizabal, R.; Singh, M.; O'Brien, T. E. Low-Cost Error Mitigation by Symmetry Verification. *Phys. Rev. A* **2018**, *98*, No. 062339.
(54) Smart, S. E.; Mazziotti, D. A. Quantum-Classical Hybrid Algorithm Using an Error-Mitigating N-Representability Condition to Compute the Mott Metal-Insulator Transition. *Phys. Rev. A* **2019**, *100*, No. 022517.
(55) McWeeny, R. Some Recent Advances in Density Matrix Theory. *Rev. Mod. Phys.* **1960**, *32*, 335−369.
(56) Ericsson, T.; Ruhe, A. The Spectral Transformation Lánczos Method for the Numerical Solution of Large Sparse Generalized Symmetric Eigenvalue Problems. *Math. Comput.* **1980**, *35*, 1251−1268.
(57) Lloyd, S.; Mohseni, M.; Rebentrost, P. Quantum Principal Component Analysis. *Nature Physics* **2014**, *10*, 631−633.
(58) LaRose, R.; Tikku, A.; O'Neel-Judy, É.; Cincio, L.; Coles, P. J. Variational Quantum State Diagonalization. *npj Quantum Inf.* **2019**, *5*, No. 57.

https://dx.doi.org/10.1021/acs.jpca.0c09530
J. Phys. Chem. A 2021, 125, 1827−1836